Journal of Heat Transfer

Technology Review

Impingement Heat Transfer: Correlations and Numerical Modeling

Neil Zuckerman
e-mail: zuckermn@seas.upenn.edu

Noam Lior
e-mail: lior@seas.upenn.edu

The University of Pennsylvania,
Department of Mechanical Engineering and Applied Mechanics,
297 Towne Building,
Philadelphia, PA 19104-6315

Uses of impinging jet devices for heat transfer are described, with a focus on cooling applications within turbine systems. Numerical simulation techniques and results are described, and the relative strengths and drawbacks of the k-ε, k-ω, Reynolds stress model, algebraic stress models, shear stress transport, and v^2f turbulence models for impinging jet flow and heat transfer are compared. Select model equations are provided as well as quantitative assessments of model errors and judgments of model suitability.
[DOI: 10.1115/1.1861921]

1 Introduction

This is a brief review of numerical methods applied to problems in impingement heat transfer with the goal to identify preferred methods of predicting and optimizing the impinging flow performance. An emphasis is on heat transfer in turbine systems. Due to page limitations the equations and governing physics will not be presented in this article, but sufficient citations are included so that interested readers could find them at the appropriate sources.

Impinging jets provide an effective and flexible way to transfer energy or mass between a surface and the fluid in various applications. Heat transfer applications include cooling of stock material during material forming processes, heat treatment [1], cooling of electronic components, heating of optical surfaces for defogging, cooling of critical machinery structures, cooling of turbine components (the focus of this paper), and many other industrial processes. Typical mass transfer applications include drying and removal of small surface particulates. General physics, uses of, and performance of impinging jets have been discussed in a number of reviews [2–5] and will only be briefly described here. Figure 1 shows the arrangement of a set of impinging jets including the various regions of flow. The flow progresses from a free jet to a stagnating jet and then turns into a wall jet. Adjacent wall jets may combine to form a fountain region.

Compared to other heat or mass transfer arrangements that do not employ phase change, the jet impingement device offers efficient use of the fluid, and high transfer rates. For example, compared with conventional convection cooling by confined flow parallel to (under) the cooled surface, impingement produces heat transfer coefficients that are up to threefold higher at a given maximum flow speed, because the impingement boundary layers are much thinner, and often the spent flow after the impingement serves to further turbulate the surrounding fluid. Given a required heat transfer coefficient, the flow required from an impinging jet device may be two orders of magnitude smaller than that required for a cooling approach using a free wall-parallel flow. For more uniform coverage over larger surfaces, multiple jets may be used. The impingement cooling approach offers a compact hardware arrangement with no additional moving parts.

In turbine applications, impinging jet flows may be used to cool several different sections of the engine such as the combustor case, combustor can walls, turbine case/liner, and the critical high-temperature turbine blades. The gas turbine compressor offers a steady flow of pressurized air at temperatures lower than those of the turbine and of the hot gases flowing around it. Typical high-pressure bleed flows used to cool the blades are available at 600°C and must cool a turbine immersed in gas of around 1400°C total temperature [6]. This requires heat transfer coefficients in the range of 1000–3000 W/m^2 K, which equates to a heat flux on the order of 1 MW/m^2. The ability to cool these components in high temperature regions and increase the cooling rates allows higher cycle temperature ratios and higher power efficiency, improving fuel economy and raising turbine power output per unit weight. Modern turbines have gas temperatures in the main turbine flow in excess of the continuous operation temperature limits of the materials used for the blades, meaning the structural strength and component life are dependent upon effective cooling.

Compressor bleed flow is commonly used to cool the turbine blades by routing it through internal passages to keep the blades at an acceptably low temperature. As shown schematically in Fig. 2, the same air can be routed to a perforated internal wall to form impinging jets directed at the blade exterior wall. Upon exiting the blade, the air may combine with the turbine core airflow. Variations on this design may combine the impinging jet device with internal fins, smooth or roughened cooling passages, and effusion holes for film cooling. Figure 3 shows a general layout of an impinging jet cooling arrangement incorporated into a double-walled combustor liner. The operation of this device depends on flow acceleration through the liner holes, driven by the compressor, and carries an associated pressure drop penalty typically in the range of 1–3% of compressor fluid pressure, depending on the degree of cooling needed. In both arrangements the designer may alter the spacing or locations of jet and effusion holes to concentrate the flow in the regions requiring the greatest cooling. Though the use of bleed air carries a performance penalty (cf. Taniguchi et al. [7]), the small amount of flow extracted has a small influ-

Contributed by the Heat Transfer Division of ASME for publication in the JOURNAL OF HEAT TRANSFER. Manuscript received February 29, 2004; revised manuscript received October 21, 2004. Review conducted by: S. Acharya.

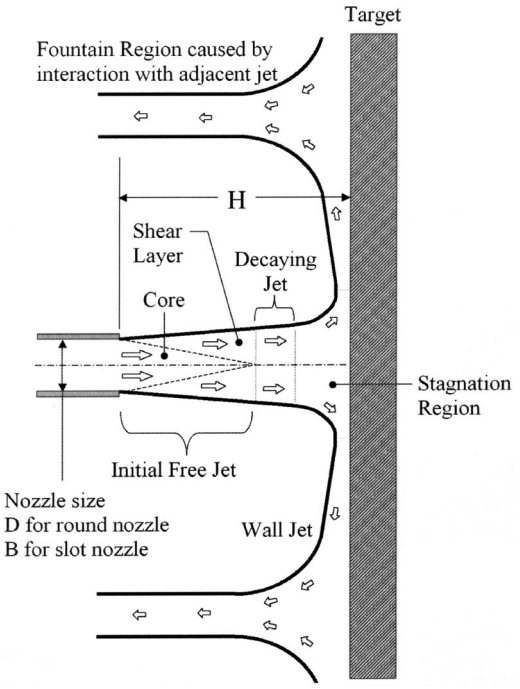

Fig. 1 The flow regions of impinging jets

ence on bleed air supply pressure and temperature. In addition to high pressure compressor air, turbofan engines provide cooler fan air at lower pressure ratios, which can be routed directly to passages within the turbine liner. A successful design uses the bleed air in an efficient fashion to minimize the bleed flow required to maintain a necessary cooling rate.

1.1 Nondimensional Heat Transfer Coefficients and Parameters. A set of common definitions and parameters are used to compare submerged impinging jet designs with a wide variety of operating temperatures, geometric scales, and fluids. The Nusselt number for jet impingement is typically defined as

$$\mathrm{Nu} = hD/k_c, \tag{1}$$

where h is the convective heat transfer coefficient defined as

$$h = \frac{-k_c \dfrac{\partial T}{\partial \vec{n}}}{T_{\mathrm{wall}} - T_{0\mathrm{jet}}} \tag{2}$$

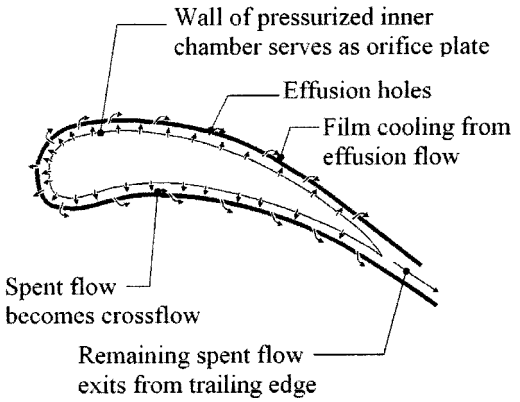

Fig. 2 Turbine blade impingement cooling flow path

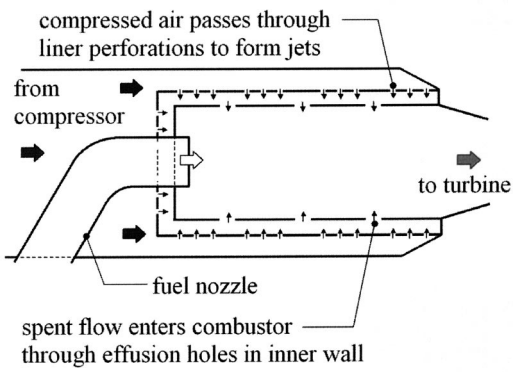

Fig. 3 Combustor section impinging-jet-cooled liner

The term $\partial T/\partial n$ gives the temperature gradient component normal to the wall.

The nondimensional parameters selected to describe the impinging jet heat transfer problem include the fluid properties such as Prandtl number Pr (the ratio of fluid thermal diffusivity to viscosity, fairly constant), plus the following:

- H/D—nozzle height to nozzle diameter ratio
- r/D—radial position from the center of the jet
- z/D—vertical position measured from the wall
- Tu—turbulence intensity, evaluated at the nozzle, $= \sqrt{\overline{u_j' u_j'}/\overline{u_i u_i}}$
- Re—jet Reynolds number $U_0 D/\nu$
- M—Mach number, based on nozzle exit average velocity (of smaller importance at low speeds, i.e., $M<0.3$)
- p_{jet}/D—jet center-to-center spacing (pitch) to diameter ratio, for multiple jets
- A_f—free area (=[total nozzle exit area/total target area]-1)
- f—relative nozzle area (=total nozzle exit area/total target area)

Jet behavior is typically categorized and correlated by its Reynolds number $\mathrm{Re}=U_0 D/\nu$, defined using initial average flow speed (U_0), the fluid viscosity (ν), and the characteristic length that is the nozzle exit diameter D or twice the slot width, $2B$ (the slot jet hydraulic diameter). At Re<1000 the flow field exhibits laminar flow properties, at Re>3000 the flow has turbulent features, and a transition regions occurs between these regimes. Turbulence has a large beneficial effect on the heat transfer rates. For example, an isolated round jet at Re=2000 (transition to turbulence), Pr =0.7, $H/D=6$ will deliver an average Nu of 19 over a circular target spanning six jet diameters, while at Re=100,000 the average Nu on the same target will reach 212 [2]. In contrast, laminar jets at close target spacing will give Nu values in the range of 2 to 20. In general, the exponent b in the relationship $\mathrm{Nu}\propto \mathrm{Re}^b$, ranges from $b=0.5$ for low-speed flows with a low-turbulence wall jet, up to $b=0.85$ for high Re flows with a turbulence-dominated wall jet.

1.2 Nozzle Design. The geometry and flow conditions for the impinging jet depend upon the nature of the target and the fluid source (compressor). In cases where the pressure drop associated with delivering and exhausting the flow is negligible, the design goal is to extract as much cooling as possible from a given air mass flow. Turbine blade passage cooling is an example of such an application; engine compressor air is available at a pressure sufficient to choke the flow at the nozzle (or perhaps some other point in the flow path). As the bleed flow is a small fraction of the overall compressor flow, the impinging jet nozzle pressure ratio will vary very little with changes in the amount of airflow

extracted. The cooling characteristics (based on flow and temperature) will instead vary greatly with changes in corrected compressor speed.

The details of the impingement device design affect the nozzle pressure drop, which then equates to a power requirement for the device. In the simplest of devices, this power is simply the volumetric flow rate multiplied by the nozzle exit dynamic pressure. In real installations, after passing over the target surface, the ''spent flow'' must exit the device. The overall power requirement then depends upon the details of the compressor intake pathway, compressor efficiency, flow path leading to the nozzle, and backpressure of the fluid exiting the target region. For this reason, one or more long, narrow supply pipes (common in experimental studies but not common to turbine designs) may not make an efficient device. Compact orifice plate nozzles have up to 2.5 times the pressure drop of a short, smooth pipe nozzle at a given mass flow and nozzle area, but provide a larger velocity gradient in the shear layer and thereby promote turbulence in the free-jet region [8]. Such orifice plates take up small volume for the hardware, are easy and inexpensive to make, and integrate well into the contoured airfoil surfaces of turbine blades. A thicker orifice plate (thickness from $0.3D$ to $1.5D$) allows the use of orifice holes with rounded entry pathways, approaching an ideal bellmouth shape, as with the contoured nozzle. This successful compromise comes at the expense of greater hardware volume and complexity, but reduces the static pressure losses to those required to accelerate the flow to the exit speed plus that of mild contraction into the rounded passageway. The orifice plate nozzle array remains the most practical and flexible geometry for turbine cooling due to its compact size and its ability to focus additional flow on regions requiring higher heat flux (e.g., blade leading edges) by variation in the nozzle hole spacing.

A series of additional holes in the fluid supply plate of an orifice array, designed for the spent flow, can provide benefits in cases with restrictive exit pathways. These effusion holes vent to exit ducting or the surroundings to provide a lower-restriction exit pathway for spent air. In a turbine blade (Fig. 2) the preferred effusion pathways are either through holes in the target wall itself (the blade exterior) to form a film cooling layer on the opposing surface, or through the confined flow region leading to aerodynamically favorable exit holes on or near the trailing edge of the blade. In highly confined flows, the use of sharp-edged nozzles and well-positioned effusion holes rather than simple pipe jets can increase Nu by a factor of 2 at a given Re, which is important in turbine cooling where jet mass flow directly affects turbine performance.

1.3 Typical Impinging Jet Device Characteristics. Typical gas jet installations for heat transfer span a Reynolds number range from 4000 to 80,000. H/D typically ranges from 2 to 12. Ideally, Nu increases as H decreases, so a designer would prefer to select the smallest tolerable H value, noting the effects of exiting flow, manufacturing and assembly capabilities, and physical constraints, and then select nozzle size D accordingly. For small-scale turbomachinery applications jet arrays commonly have D values of 0.2–2 mm, while for larger scale industrial applications, jet diameters are commonly in the range of 5–30 mm.

2 Prediction and Modeling of Impinging Jet Performance

The designer of an impinging jet device needs to predict the transfer coefficient profile (Nu), necessary fluid flow per unit of target area (G), and pressure drops in advance of manufacturing the hardware. Accurate models or calculation methods are desirable as they minimize the amount of testing required. A reliable set of models provides the designer with a rapid, inexpensive, and flexible alternative to conducting a series of hardware tests. Modeling of the turbulent flow, incompressible except for the cases where the Mach number is high, is based on using the well-established mass, momentum, and energy conservation equations.

2.1 Empirical Correlations. First, simple correlations such as those supplied by Martin [2] (with a summary in Ref. [1]) predict Nu as a function of the governing parameters (as listed in Sec. 1.1) in cases where the fluid has a continuously laminar flow over the entire fluid and target region of interest ($\mathrm{Re}_{jet} < 1000, \mathrm{Re}_{wall} < 10{,}000$). A list of available impingement heat transfer correlations for laminar and turbulent flows is presented in the Appendix.

2.2 Laminar Impingement. For laminar flows in many geometries, the governing equations may be reduced to analytical solutions, such as that for a stagnating flow field placed above a wall boundary layer [9]. Numerical modeling of steady laminar flows is fairly straightforward, using the mass, momentum, and energy conservation equations in time-invariant forms. This simulation approach may even yield useful results for flows which are laminar over most but not all of the domain. Kang and Greif [10] successfully predicted flow field properties, separation locations, and heat transfer coefficients for impinging jets on cylinders for $100 \leqslant \mathrm{Re} \leqslant 1000$, including exploration of buoyancy effects.

2.3 Turbulent Impingement Models. Most impinging jet industrial applications involve turbulent flow in the whole domain downstream of the nozzle, and modeling turbulent flow presents the greatest challenge in the effort to rapidly and accurately predict the behavior of turbulent jets. Numerical modeling of impinging jet flows and heat transfer is employed widely for prediction, sensitivity analysis, and device design. Finite element, finite difference, and finite volume computational fluid dynamics (CFD) models of impinging jets have succeeded in making rough predictions of heat transfer coefficients and velocity fields. The difficulties in accurately predicting velocities and transfer coefficients stem primarily from modeling of turbulence and the interaction of the turbulent flow field with the wall.

The computation grid must resolve both the upstream and downstream flow around the nozzles or orifices and must extend sufficiently far to the side of a single jet or array (typically 8–10 diameters) to provide realistic exit conditions. Zero-gradient and constant-static-pressure conditions have been used at the far-field model boundaries. Successful, stable modeling using both of these conditions can depend on properly shaping the boundary at the edge of the model domain. Turbulent impinging jet CFD employs practically all available numerical methods, which will be critically and briefly reviewed below. For brevity the governing equations are not listed here. Full equation sets for each model are available in the referenced publications.

2.3.1 DNS and LES. The direct numerical simulation (DNS) method solves the full Navier–Stokes, continuity, and energy/mass diffusion equations using discrete units of time and space, but requires an extremely small grid to fully resolve all the turbulent flow properties, because the microscopic turbulent length scales involved in jet impingement are far smaller than the macroscopic lengths involved (e.g., D_0 or H). The consequently long computation time practically limits the use of DNS to Reynolds numbers much lower than those in the gas turbine impingement heat transfer application. In an attempt to remedy this situation, some CFD models use large eddy simulation (LES). The time-variant LES approach tracks flow properties with the full equations down to some user-defined length scale (typically the grid spacing), and then uses additional subgrid-scale equations to describe turbulent flow behavior at smaller scales. The LES method has shown encouraging results and clarified the understanding of formation, propagation, and effects of flow eddies upon the velocity fields and jet transfer characteristics [11–14], but it requires high resolution in space for accuracy, may require high resolution in time for stability and accuracy, and therefore still needs a great amount of computing power or time to produce satisfactory solu-

tions for the transitional and turbulent flows of interest here (Re >1000). LES modeling by Cziesla et al. [15] demonstrated the ability of LES to predict local Nu under a slot jet within 10% of experimental measurements. The use of LES does not necessarily have an upper or lower limit on Re (though particular codes may be limited to $M \leqslant 1$), but for laminar flows ($\mathrm{Re} < 1000$) the influence of turbulence is small enough that the DNS approach offers little improvement in accuracy over the time-averaged techniques detailed below. For those cases where computational cost is not a primary concern, the LES method offers the greatest information about the impinging jet flow field.

2.3.2 The RANS Approach. Steady-state time-averaged solution techniques, typically Reynolds-averaged Navier–Stokes (RANS) models, use some version of the Navier–Stokes equations adjusted for the presence of turbulent flow. The majority of RANS models used for jet flows fit into one of two categories, the eddy-viscosity models and the computationally more costly full second moment closure (SMC) models. Eddy viscosity models treat the turbulent viscosity as a scalar quantity, assuming or forcing an isotropy in the normal stresses [16]. The various full SMC models track all Reynolds stresses or track the various components of a nonuniform turbulent viscosity. These models approximate the Reynolds stresses and heat fluxes using semi-empirical equations based on expected physical trends rather than direct derivations. The semi-empirical equations provide approximations of undetermined terms within the second-moment equations, typically two-parameter correlations. With further manipulation a series of higher-order-moment equations can be generated, but these more complex models have even more correlation terms and unknowns, which require approximate modeling.

2.3.3 Near-Wall Treatment. In addition to the portions of the CFD model describing the fluid flow inside the computational domain, the steady and transient models require a description of how the flow behaves next to the wall (the target surface). This part of the model typically plays the major role in properly predicting both the flow and the heat transfer [17]. The fundamental difficulty comes from the need to describe how the turbulent regions of a decelerating flow field interact with the wall, including in the wall's boundary layer. A variety of often very different wall damping and reflection terms have been implemented. Numerical solutions have shown that heat transfer rates within the viscous sublayer are of a larger magnitude than outside the layer. The spatial region in which the turbulence models have the greatest difficulty approximating the flow is the same region in which the largest heat and mass gradients occur, and so this region cannot be neglected.

Numerical models of turbulence near the wall commonly feature one of two approaches. In the first obvious approach, the grid near the wall is constructed at sufficiently high resolution to properly resolve flow in the entire viscous sublayer and turbulent boundary layer with turbulence equations intended for use at low cell Reynolds numbers. This requires a model capable of resolving turbulent behaviors very close to the wall, and a large computation effort.

The alternate method uses algebraic equations to relate steady and fluctuating velocity and scalar profiles to wall distance and surrounding fluid properties. These wall functions predict the flow properties in and above the viscous sublayer. This method requires only a single cell in the sublayer, and thus requires less computational time. Relations for high Re parallel flows such as the "law of the wall" are based upon flows in different geometry than that of the impinging jet and may not produce a correct velocity profile near the wall, especially in cases where the flow separates or reverses on the target surface. The standard law of the wall is based upon the absence of pressure gradients near or along the wall, clearly a different flow field than that seen in the stagnation region of an impinging jet. The nonequilibrium law of the wall is based upon differing turbulent energy generation and destruction rates and accounts for pressure gradients. Bouainouche et al. [18] performed modeling with various wall equations and concluded that the standard logarithmic law of the wall poorly predicted shear stresses (errors of up to -30% in the stagnation region) and that a generalized nonequilibrium law of the wall performed well in the stagnation region but under predicted wall shear stress in the wall-jet region (errors of up to -12%). Their "hybrid law of the wall" model produced improved results by using the nonequilibrium law in the stagnation region and switching to the logarithmic law in the wall-jet region.

Specific difficulties arise with the numerical modeling of impinging jets. A number of models reviewed below, such as k-ε, have been optimized for free-shear flows such as submerged jets. Some models, such as k-ω, perform best in boundary-layer flows such as the wall-jet region. Unfortunately, the impinging jet problem contains both of these as well as significant pressure gradients in the stagnation region. The normal strain and the rise in fluid pressure in the stagnation region affect the turbulent flow through distinct terms in the second-moment RANS equations. The pressure plays a part in the turbulent diffusion term. The effects of changing pressure play an even greater role in the pressure-strain rate correlation term. Unlike the turbulent diffusion term, which most models focus on approximating, the pressure-strain correlation was usually of secondary interest. As a result, most models have simpler and less accurate predictions for turbulent effects in the stagnation region. A wide variety of equation sets have been implemented to model these pressure-strain rate correlation terms related to $\nabla u'$ and ∇u, with varying success. The two equation eddy-viscosity models, such as k-ε, contract the rank-2 tensors in the equations to eliminate terms, and thus drop these terms. That is, the two-equation models are based around assumptions about the low importance of pressure gradients and the minimal anisotropy of the Reynolds stresses, and experiments have shown that these modeling assumptions do not apply in the stagnation region.

2.3.4 The Boussinesq Approximation. The simplified RANS models need some approximation to determine the Reynolds stresses. An equation known as the Boussinesq approximation (or hypothesis) describes a simple relationship between turbulent stresses and mean strain rate. Given a strain rate tensor S_{ij}, where $S_{ij} = 1/2[(\partial \overline{u_i}/\partial x_j) + (\partial \overline{u_j}/\partial x_i)]$ the approximation gives a formula for the Reynolds stress tensor

$$-\rho \overline{u_i' u_j'} = 2\mu'(S_{ij} - \tfrac{1}{3} S_{kk}\delta_{ij}) - \tfrac{2}{3}\rho k \delta_{ij} \tag{3}$$

By itself, the Boussinesq approximation does not constitute a complete turbulence model, as the value of μ' is unknown and depends on turbulence scales unique to each problem.

2.3.5 The k-ε Model. The commonly tested "k-ε" eddy-viscosity model is widely acknowledged as producing poor results in the impinging jet problem, but remains a benchmark against which to compare better models [17]. The k-ε model remains in use due to its common implementation and comparatively low computational cost. The model uses the Boussinesq hypothesis to calculate the Reynolds stresses as a direct function of the velocity gradients and is based on flow behavior at higher Reynolds numbers (fully turbulent fluid flow). It independently tracks turbulent energy k and turbulence destruction or dissipation rate ε, with a dissipation equation based upon expected trends. As with most RANS models it requires experimentally determined constants to fully close the equations. The k-ε model can produce acceptable results for free-shear flows but provides poor simulation of wall-jet flows. The model requires the user to specify ε at each boundary, but at the walls ε has a finite, nonzero value that is not known in advance. For the impinging jet problem it gives useful results in the free-jet region but poor results in the stagnation region and wall jet region, as detailed below. It gives poor predictions of the location of separation points on solid boundaries and for the impinging jet problem it may fail to predict the occurrence of secondary peaks in Nu. The standard k-ε model is formulated for

flows at high Reynolds number and does not apply in regions where viscous effects on the flow field are comparable in magnitude to turbulent effects (such as in the sublayer next to a wall). In many cases the model uses wall functions to determine the velocity profiles. Alternately, k-ε models have been built with additional terms and damping functions to allow the model to simulate portions of the flow at low Reynolds numbers.

The Launder and Sharma low Reynolds number model used by Craft et al. [17] in a comparative CFD study of various turbulence models used for the impinging jet problem incorporates conservation equations for k and ε as well as a simple equation to set the velocity-temperature correlation (heat flux) proportional to the temperature gradient. This version of the model includes the Yap correction term to adjust the dissipation rate $\tilde{\varepsilon}$ as a function of k, $\tilde{\varepsilon}$, and distance from the wall y. At low Re a damping function is used to add an adjustment to the turbulent viscosity used in the conservation equations. It increases the dissipation to reduce the turbulent length scale. Without the correction the model will over predict turbulent length scale and overpredict turbulent viscosity. The model constants depend on empirical data, and the correction terms and associated constants are therefore somewhat arbitrary, so engineers continually invent alternate adjustment terms with different closure coefficients.

Heyerichs and Pollard [19] conducted a numerical comparison of three different wall function and five different wall damping functions with an impinging jet test case and concluded that the selected k-ε models with wall functions gave consistently poor results, with Nu errors in the range of -21.5–-27.8% in the stagnation region, and $+32$–$+38.4\%$ at the secondary peak. Somewhat better matches were produced using models with damping functions, but those models still produced errors in Nu of up to 50% and misplaced the secondary peak. They concluded that basing the damping functions on wall position y^+ caused the poor results, as the damping functions using y^+ were based upon simple wall-parallel flows with simple boundary layers, rather than the flow found in the stagnation region of the impinging jet.

Craft et al. [17] presented a comparison of a two-dimensional implementation of the k-ε model versus test data. For the test case at Re=23,000 the model predicted centerline wall-normal-root-mean-square (rms) velocity levels up to four times larger than those measured in the experimental work of Cooper et al. [20]. A specific problem noted in the k-ε model was that the model equation relating turbulent kinetic energy to turbulent viscosity caused increasing and erroneous turbulent kinetic energy levels in the stagnation region (increasing turbulent viscosity caused increasing turbulence intensity). The model similarly over predicted wall normal r.m.s. velocity at $r/D=0.5$, corresponding to the edge of the jet. Wall-parallel velocity errors were in the range of 15–20%, with errors of up to 50% in the $y/D<0.05$ region very close to the wall. The model over predicted Nu in the center of the impingement region by up to 40% and failed to predict the secondary Nu peak at $r/D=2$. Craft et al. [21] continued work with this type of model, developing an alternate k-ε model which produced greatly improved impingement centerline wall-normal fluctuating velocity values and better Nu predictions in the $r/D<2$ region. The largest errors in Nu were typically 15%, occurring in the range of $1<r/D<3$. Turgeon and Pelletier [22] built adaptive k-ε models which succeeded in generating a solution with minimal grid dependence, showing that the difficulties with applying the k-ε model are independent of grid resolution and persist for small mesh sizes. Merci et al. [23] devised and tested an altered nonlinear variation of the k-ε model, yielding improved results over the standard model but an under prediction of $\mathrm{Nu}/\mathrm{Nu}_0$ of up to 25% (alternately interpreted as an over prediction of Nu_0). Souris et al. [24] showed that the upstream errors in low Reynolds number k-ε model predictions resulted in large downstream errors, giving wall-jet thicknesses up to double that of experiment, and wall-jet peak velocity as much as 44% below experimental results. From the various studies conducted, we conclude that the even the best k-ε models and associated wall treatments will yield Nu profiles with local errors in the range of 15–30%, and the standard k-ε model is not recommended for use in the impinging jet problem. These shortcomings are attributed to the assumption of isotropic turbulence and the use of wall functions that poorly approximate near-wall velocity fluctuation and associated transport properties.

2.3.6 The k-ε RNG Model. Other variations of the model have been applied, such as the renormalization group theory k-ε model (RNG). The RNG model incorporates an additional term in the turbulent energy dissipation equation based on strain rates, and includes adjustments for viscous effects at lower Re and a calculation of turbulent Pr. Heck et al. [25] showed the RNG model provided a close match of Nu in the wall-jet region but an error of up to 10% in the stagnation region. This is in part due to the RNG model's tendency to predict jet spreading rates that are as high as twice that found in experiment [26]. This flaw on the upstream end of the model leads one to question how the downstream results did not stray as far from measured values. It offers some improved performance over the standard k-ε at a slightly higher computational cost and is recommended when only moderate accuracy is required.

2.3.7 The k-ω Model. The k-ω model solves for turbulent kinetic energy (k) and energy dissipation rate per unit of turbulent kinetic energy (ω), where ω is determined through a conservation equation including experimentally determined functions, rather than direct calculation from the velocity field [26]. The equations for ω treat it as a vorticity level or vortex fluctuation frequency. The model then produces turbulent viscosity as a function of k and ω.

As with the k-ε model, the latest versions of the k-ω model include correction terms to improve predictions in the low Reynolds number flow regions. The k-ω model typically produces Nu profiles with a local error of up to 30% of the experimental Nu value. It can produce better predictions of the turbulent length scale than the k-ε model. The k-ω model can generate good predictions of flow properties in the wall jet, both in the sublayer and logarithmic region, without the need for damping functions. For a flow near a wall the boundary conditions are known—turbulent viscosity and the turbulent time scale are set to zero. The value of ω at or near the wall-adjacent cell may be set proportional to ν/y^2, meaning the user can fully specify the turbulence conditions at the wall, unlike in the k-ε model. Unfortunately the k-ω model is sensitive to far-field boundary conditions, much more so than the k-ε model. Park et al. [27] demonstrated some improved results using the k-ω equations but noted that at higher Re (25,100) the secondary Nu peaks appeared too far inward, as low as 50% of the experimentally measured value of x/B. The local levels of Nu were overpredicted by as much as 100% as the result of misplacing this peak. A comparative study by Heyerichs and Pollard [19] found that the k-ω model over predicted Nu by up to 18% and generated a secondary peak closer to the jet center than found in experiment, but concluded that for the impinging jet problem it clearly outperformed the nine different implementations of the k-ε model used in the study. The low-Re k-ω model gave good results by matching the shape of the experimental curves, but alternate formulations of the impinging jet CFD model using k-ω with wall functions gave poor results—they replaced the k-ω model with a cruder approximation in the very region where it gives the best results, overpredicting wall jet Nu by as much as 40%. Chen and Modi [28] successfully applied the k-ω model for mass transfer at high Sc, and claimed agreement within 10% of experimental results, given very high grid densities. The addition of cross-diffusion terms in various k-ω models have succeeded in reducing its sensitivity to far-field ω boundary conditions, a problem known to arise during use of the k-ω model for unconfined or partially confined flows. With the inaccurate free-jet modeling, dense wall grid requirement, and undesirable sensitivity

to unknown far-field conditions, we conclude the k-ω model is only moderately better than the k-ε; it offers better predictions of Nu, with a higher computational cost.

2.3.8 Realizability Constraints. In cases of high strain rate the simple Boussinesq approximation may predict negative normal Reynolds stresses or excessively high Reynolds shear stresses. The k-ε, k-ω, and v^2f models described herein have been commonly modified to use realizability limits to prevent these problems. A common fix is to allow variation in the constant of proportionality C_μ found in the turbulent viscosity equation $\nu' = C_\mu(k^2/\varepsilon)$ [29]. Physical measurements have demonstrated variation in this ''constant'' in differing fluid flows. Other approaches put simple limits on time scales, length scales, strain rates, and/or terms including strain rates.

Abdon and Sunden [30] used nonlinear k-ε and k-ω models with realizability constraints to model impinging jets. These model adjustments produced results closer to experimental data, with the realizable k-ε model predicting Nu_0 within 10% (within the experimental data scatter) and the realizable k-ω model over predicting Nu_0 by 20%. Further studies with nonlinear versions of the k-ε and k-ω models produced Nu profiles with errors equal to or greater than the standard linear models. The nonlinear models captured a secondary peak in Nu in the proper location at $r/D = 2$, but overpredicted the Nu value by up to 50%. Park and Sung [31] constructed a k-ε-f_μ model for low Re flows, where the turbulent viscosity damping function f_μ incorporated terms to describe damping near the wall and terms to describe the equilibrium flow farther from the wall. With the inclusion of realizability limits on eddy viscosity they were able to improve the Nu profile predictions for $r/D < 1.5$ to within 10–20% of experimental results, primarily by limiting overprediction of turbulent kinetic energy in the jet center. For the region of $r/D < 1$ the model was tuned to predict the Nu profile within 15%, giving a flat profile matching the experimental results. Given the slightly higher computational cost but potentially better results, realizability constraints are recommended for use in impinging jet flow CFD.

2.3.9 Algebraic Stress Models. Algebraic stress models (ASM) can provide a computationally inexpensive approach valid for some simple flows. The ASM models may be built with lower grid resolution in the wall region which contributes to the computational efficiency. Rather than solve complete discretized differential transport equations this category of models solves algebraic equations which require fewer calculations. In cases where the turbulent velocity fluctuations change slowly compared to changes in the mean velocity, the Reynolds stresses can be approximated as algebraic functions of the dominant mean velocity derivatives in time and space. In a simple case the ASM may use equations for calculating a length scale which are particular to the problem geometry. This length scale is used to calculate turbulent viscosity, which is used with the Boussinesq approximation to determine the Reynolds stresses. Use of this approach requires enough advance knowledge of turbulent length and time scales for the problem of interest that the quantities may be calculated using algebraic equations, a potential source of large error. For simple geometries such as pipe flow or free jets a set of equations for mixing length are available. Some ASMs simply drop the time and space derivatives of the Reynolds stresses from the equations, leaving only gradients of the mean flow velocity [32]. This approach assumes the turbulent convection and turbulent diffusion effects either are insignificant or balance each other. Unfortunately, for the impinging jet problem the boundary layer along the wall is not in equilibrium and this type of ASM is a crude approximation.

Comparative modeling by Funazaki and Hachiya showed that for an impingement problem their ASM overpredicted Nu by approximately 30%, outperforming k-ε and RNG k-ε models which typically showed 50–55% error [33]. Numerical work by Souris et al. [24] found that the ASM had better free-jet modeling than the k-ε model, which generated better results in the wall region downstream. Both models over predicted the centerline velocity decay but the ASM over prediction was not as high. The error in jet width prediction of the ASM was as high as 35% close to the wall, better than the 59% error produced by the low Reynolds number version of the k-ε model. This ASM model used the standard logarithmic law of the wall and generated poor predictions of velocity profile in the region closest to the wall (within the first quarter of the wall-jet thickness), with high jet thicknesses (up to 65% error at $r/D = 2.5$) and wall jet velocity magnitudes as much as 45% below experiment. These results do not mean the ASM correctly described the impinging flow, but rather the k-ε model resulted in gross errors, larger than the errors present when using the ASM. The ASM may be better than a number of poor k-ε models, but is not recommended as it does not yield high accuracy.

2.3.10 Complete RSM Modeling. The SMC Reynolds stress model (RSM), also known as the Reynolds stress transport model (RSTM), independently tracks all six components of the rank-2 Reynolds stress tensor, accounting for production, diffusive transport, dissipation, and turbulent transport. Common implementations require a number of constants to resolve terms such as a pressure-strain term and terms in the turbulence dissipation equation. Because the RSM model does not assume isotropic stresses it can give much better predictions of fluid behavior in turning or rotating flows that those of the two-equations models.

RSM modeling of impinging jets by Demuren [34] showed velocity predictions ranging from -40% to $+40\%$ of the experimentally measured velocities, and Reynolds Stress errors of over 100%, which was attributed to a need for an extremely dense grid (denser than that utilized in the modeling). Craft et al. [17] presented computed centerline wall-normal rms turbulent velocity levels, which matched within 25% of experiment at $H/D = 2$, but had errors as large as 80–100% for $H/D = 6$. The RSM can predict the occurrence of a secondary peak in Nu but not necessarily at the correct location [35]. This shows that although the various RSM implementations preserve all the Reynolds stress terms, they still use approximation equations based on a number of assumptions. That is, they eliminate the isotropy assumptions which yield the two-equation models but still rely upon other empirically generated equations to predict the stresses and do not give a ''perfect'' solution. Given the high computational cost compared to the eddy-viscosity models, these results are disappointing and the RSM is not recommended as an alternative.

2.3.11 The v^2f Model. Durbin's v^2-f model, also known as the ''normal velocity relaxation model,'' has shown some of the best predictions to date, with calculated Nu values falling within the spread of experimental data [36,37]. The v^2-f model uses an eddy viscosity to increase stability (rather than using a full RSM) with two additional differential equations beyond those of the k-ε model, forming a four-equation model. It uses the turbulent stress normal to the streamlines (referred to as $\overline{v^2}$) to determine the turbulent eddy viscosity, rather than the scalar turbulence intensity used in the k-ε model. It incorporates upper and lower limits on the turbulent time and length scales. In some implementations the limits on these terms have been further modified to impose realizability constraints [38].

As with the k-ω model, the v^2f model requires a dense wall grid. In some cases the v^2-f model has been shown to predict realistic levels of turbulence in the decelerating jet core but excessive turbulence levels in the shearing flow outside the core and in the wall jet [39]. Despite this difficulty and its moderately high computational cost, it is acknowledged as one of the best predictors of Nu distribution. It has an advantage over the standard k-ε series of models because it can predict the occurrence, position, and magnitude of the secondary Nu peak for low H/D. This

Table 1 Comparison of common CFD turbulence models used for impinging jet problems. The relative performance of the various models is rated qualitatively on a scale from "*" indicating undesirable model characteristics, to "**" indicating excellent model characteristics.**

Turbulence Model	Computational cost (computation time required)	Impinging jet transfer coefficient prediction	Ability to predict secondary peaks in Nu
k-ε	**** Low cost	* Poor: Expect Nu errors of 15–60%	* Poor
k-ω	**** Low-moderate	** Poor-fair: Anticipate Nu errors of at least 10–30%	** Fair: May have incorrect location or magnitude
Realizable k-ε and other k-ε variations	**** Low	** Poor-fair: Expect Nu errors of at 15–30%	** Poor-fair: May have incorrect location or magnitude
Algebraic stress model	**** Low	** Poor-fair: Anticipate Nu errors of at least 10–30%	* Poor
Reynolds stress model (full SMC)	** Moderate-high	* Poor: Anticipate Nu errors of 25–100%	** Fair: May have incorrect location or magnitude
SST	*** Low-moderate	*** Good: Typical Nu_0 errors of 20–40%	** Fair
v^2f	*** Moderate	**** Excellent: Anticipate Nu errors of 2–30%	**** Excellent
DNS/LES time-variant models	* Extremely high	**** Good-excellent	**** Good-excellent

model is highly recommended for the impinging jet problem, and its moderate computational cost is offset by its ability to closely match experimental results.

2.3.12 Hybrid Modeling. The impinging jet problem has at least three distinct flow regions with distinct flow physics. The computationally efficient two-equation models discussed previously are adjusted to perform best in one physical situation, with closure equations and coefficients based on a set of simple turbulent flows. Application to alternate geometries demonstrates the weakness of each model. No simple model has produced the ultimate answer, but by combining two or more models the CFD code can produce a compromise. For example, the model may calculate in which region the flow lies (free jet, stagnation, or wall jet) and use a model successfully tested for that particular region. The solution from the multiple models in multiple regions must then be combined at the boundaries in a smooth fashion to produce a hybrid turbulence model. In doing so the CFD program may utilize the strengths and minimize the weaknesses of each model.

Menter's shear stress transport (SST) model is one of the more successful hybrid models [40]. The SST model combines the k-ω model near the wall and the k-ε model farther from the wall to utilize the strengths of each. Smooth transition between the two is accomplished by use of a blending or weighting function based upon distance from the wall. Menter's SST model uses a variant equation for determining turbulent viscosity incorporating a number of limits, with the goal of improving predictions of turbulence in adverse pressure gradients. The SST model still requires a finely spaced mesh near the wall to produce accurate results. Validation comparisons by Esch et al. [41] showed Nu predictions within 20% of experimental results, and a Nu profile no farther than 5% above or below the profile predicted by the v^2-f model. The SST model also predicted mean velocities well, clearly better than the k-ε model and within the uncertainty of the experimental measurements. This indicates the SST model may provide predictions as good as those of the v^2-f model but at a lower computational cost, and it is recommended for this reason.

2.4 Numerical Modeling Validation by Experiments. Ultimately, all CFD results should be validated by comparison to reliable experimental results and to determine overall model error in predicting the real situation. Obviously, the model should match the experimental conditions, including all of the geometry, fluid entry, exit conditions, and target surface properties. This matching must include not only the domain boundary average velocities, pressures, and temperatures, but also their turbulent components.

3 Conclusions and Recommendations

A large number of informative studies have been conducted using the k-ε model to attempt to predict the heat/mass transfer of impinging jets, with only limited success. Examination of RANS numerical modeling techniques showed that even with high-resolution grids, the various implementations of the k-ε, k-ω, RSM, and ASM models give large errors compared to experimental data sets. The v^2f and SST models can produce better predictions of fluid properties in impinging jet flows and are recommended as the best compromise between solution speed and accuracy. Modeling work conducted by the authors indicates the v^2f model will provide more accurate predictions than the SST model. Table 1 summarizes the relative performance of the various models.

The review of recent impinging jet research publications identified a particular need of the engineering design community. Specifically, it needs a turbulence model, and associated wall treatment (if necessary), that reliably and efficiently provides time-averaged transfer coefficients for impinging jet flowfields. Given

the varied and inaccurate results of the alternatives, the SST and v^2-f models offer the best results for the least amount of computation time. Even so, they are imperfect. The improved turbulence model must correctly predict the jet spreading, turbulent flow effects in the stagnation region, and turbulent flow properties along the wall. Though inelegant, the solution by means of a hybrid model would serve this purpose if it included a turbulence model carefully adjusted to properly simulate the turning anisotropic flow field in the stagnation region.

Nomenclature

A_f = target free area
b = correlation exponent, used in $\mathrm{Nu} \propto \mathrm{Re}^b$
B = slot jet nozzle width
c_p = specific heat of fluid
D = nozzle diameter
D_h = hydraulic diameter of nozzle
f = relative nozzle area or v^2f model function
G = jet mass flow per unit of target area
h = heat transfer coefficient
H = nozzle-to-target spacing (nozzle height)
k_c = fluid thermal conductivity
k = turbulent kinetic energy
M = Mach number
n = length in wall-normal direction
Nu = Nusselt number
$\mathrm{Nu}_{\mathrm{avg}}$ = area-averaged Nusselt number
Nu_0 = Nusselt number at stagnation point
p = fluid pressure
p_{jet} = jet pitch (center-to-center distance)
Pr = Prandtl number = fluid thermal diffusivity/fluid viscosity
q'' = heat flux
Re = Reynolds Number ($=U_0D/\nu$ for a jet)
r = radial position measured from center of jet axis
Sc = Schmidt number = fluid kinematic viscosity ν/species (mass transfer) diffusivity
S_{ij} = strain rate tensor
t = time
T = temperature
$T_{0\mathrm{jet}}$ = jet adiabatic wall temperature, exiting nozzle
T_{wall} = wall surface temperature
Tu = turbulence intensity (equal to square root of [turbulent kinetic energy divided by mean kinetic energy])
U or u = fluid velocity (overbar indicates average, prime indicates fluctuating portion)
U_0 = jet initial speed, average
x = coordinate direction
y = distance from wall referenced in CFD models (normalized to "y^+" using friction velocity)
z = axial position or height, measured off of target surface
δ_{ij} = identity tensor
ε, $\tilde{\varepsilon}$ = turbulent kinetic energy dissipation rate
μ = fluid viscosity
ν = fluid kinematic viscosity
ρ = fluid density
σ_{ij} = steady stress tensor
τ_{ij} = turbulent stress tensor (Reynolds stress tensor)

Appendix: Correlation Reference in Table 2

Table 2 Correlation sets

Source	Nozzle type	Provides	Reynolds number, nozzle height range
Goldstein and Behbahani [42]	Single round nozzle	$\mathrm{Nu}_{\mathrm{avg}}$	$35{,}200 \leq \mathrm{Re} \leq 120{,}500$ $H/D = 6$ *or* 12
Goldstein et al. [43]	Single round nozzle	$\mathrm{Nu}_{\mathrm{avg}}$	$61{,}000 \leq \mathrm{Re} \leq 124{,}000$ $2 \leq H/D \leq 12$
Lytle and Webb [44]	Single round nozzle	Nu_0 and $\mathrm{Nu}_{\mathrm{avg}}$	$3600 \leq \mathrm{Re} \leq 27{,}600$ $0.1 \leq H/D \leq 1$
Martin [2]	Single round nozzle	$\mathrm{Nu}_{\mathrm{avg}}$	$2000 \leq \mathrm{Re} \leq 400{,}000$ $2 \leq H/D \leq 12$
Meola et al. [45]	Single round nozzle	$\mathrm{Nu}_{\mathrm{avg}}$	$10{,}000 \leq \mathrm{Re} \leq 100{,}000$ $10 \leq H/D$
Mohanty and Tawfek [46]	Single round nozzle	Nu_0	$4860 \leq \mathrm{Re} \leq 34{,}500$ $6 \leq H/D \leq 58$
Tawfek [47]	Single round nozzle	$\mathrm{Nu}_{\mathrm{avg}}$	$3400 \leq \mathrm{Re} \leq 41{,}000$ $6 \leq H/D \leq 58$
Wen and Jang [48]	Single round nozzle	$\mathrm{Nu}_{\mathrm{avg}}$	$750 \leq \mathrm{Re} \leq 27{,}000$ $3 \leq H/D \leq 16$
Martin [2]	Single slot nozzle	$\mathrm{Nu}_{\mathrm{avg}}$	$3000 \leq \mathrm{Re} \leq 90{,}000$ $2 \leq H/(2B) \leq 10$
Chan et al. [49]	Single slot nozzle (convex target)	Nu_0	$5600 \leq \mathrm{Re} \leq 13{,}200$ $2 \leq H/B \leq 10$
Florschuetz et al. [50]	Array of round nozzles (inline orifice nozzles)	$\mathrm{Nu}_{\mathrm{avg}}$	$2500 \leq \mathrm{Re} \leq 70{,}000$ $1 \leq H/D \leq 3$
Gori and Bossi [51]	Single slot nozzle (on cylinder)	$\mathrm{Nu}_{\mathrm{avg}}$	$4000 \leq \mathrm{Re} \leq 20{,}000$ $2 \leq H/B \leq 12$
Huber and Viskanta [52]	Array of round nozzles	$\mathrm{Nu}_{\mathrm{avg}}$	$3400 \leq \mathrm{Re} \leq 20{,}500$ $0.25 \leq H/D \leq 6$
Martin [2]	Array of round nozzles	$\mathrm{Nu}_{\mathrm{avg}}$	$2000 \leq \mathrm{Re} \leq 100{,}000$ $2 \leq H/D \leq 12$
San and Lai [53]	Array of round nozzles (staggered orifice nozzles)	Nu_0	$10{,}000 \leq \mathrm{Re} \leq 30{,}000$ $2 \leq H/D \leq 6$
Goldstein and Seol [54]	Row of round nozzles (square orifice)	$\mathrm{Nu}_{\mathrm{avg}}$	$10{,}000 \leq \mathrm{Re} \leq 40{,}000$ $0 \leq H/D \leq 6$
Martin [2]	Array of slot nozzles	$\mathrm{Nu}_{\mathrm{avg}}$	$1500 \leq \mathrm{Re} \leq 40{,}000$ $1 \leq H/(2B) \leq 40$

References

[1] Ferrari, J., Lior, N., and Slycke, J., 2003, ''An Evaluation of Gas Quenching of Steel Rings by Multiple-jet Impingement,'' J. Mater. Process. Technol., **136**(1-3), pp. 190–201.

[2] Martin, H., 1977, ''Heat and Mass Transfer between Impinging Gas Jets and Solid Surfaces,'' Adv. Heat Transfer, **13**, pp. 1–60.

[3] Jambunathan, K., Lai, E., Moss, M. A., and Button, B. L., 1992, ''A Review of Heat Transfer Data for Single Circular Jet Impingement,'' Int. J. Heat Fluid Flow, **13**(2), pp. 106–115.

[4] Donaldson, C. D., and Snedeker, R. S., 1971, ''A Study of Free Jet Impingement. Part 1. Mean Properties of Free and Impinging Jets,'' J. Fluid Mech., **45**(2), pp. 281–319.

[5] Viskanta, R., 1993, ''Heat Transfer to Impinging Isothermal Gas and Flame Jets,'' Exp. Therm. Fluid Sci., **6**, pp. 111–134.

[6] Han, J.-C., Dutta, S., and Ekkad, S., 2000, *Gas Turbine Heat Transfer and Cooling Technology*, Taylor and Francis, New York.

[7] Taniguchi, H., Miyamae, S., Arai, N., and Lior, N., 2000, ''Power Generation Analysis for High Temperature Gas Turbine in Thermodynamic Process,'' AIAA J., **16**, pp. 557–561.

[8] Lee, J., and Lee, S, 2000, ''The Effect of Nozzle Configuration on Stagnation Region Heat Transfer Enhancement of Axisymmetric Jet Impingement,'' Int. J. Heat Mass Transfer, **43**, pp. 3497–3509.

[9] Burmeister, L. C., 1993, *Convective Heat Transfer*, Wiley, New York.

[10] Kang, S. H., and Greif, R., 1992, ''Flow and Heat Transfer to a Circular Cylinder with a Hot Impinging Jet,'' Int. J. Heat Mass Transfer, **35**, pp. 2173–2183.

[11] Beaubert, F., and Viazzo, S., 2002, ''Large Eddy Simulation of a Plane Impinging Jet,'' C. R. Mecanique, **330**, pp. 803–810.

[12] Gao, S., and Voke, P. R., 1995, ''Large-eddy Simulation of Turbulent Heat Transport in Enclosed Impinging Jets,'' Int. J. Heat Fluid Flow, **16**, pp. 349–356.

[13] Hällqvist, T., 2003, ''Numerical Study of Impinging Jets with Heat Transfer,'' Licentiate Thesis, Royal Institute of Technology, Stockholm, Sweden.

[14] Olsson, M., and Fuchs, L., 1998, ''Large Eddy Simulations of a Forced Semi-confined Circular Impinging Jet,'' Phys. Fluids, **10**(2), pp. 476–486.

[15] Cziesla, T., Biswas, G., Chattopadhyay, H., and Mitra, N. K., 2001, ''Large-Eddy Simulation of Flow and Heat Transfer in an Impinging Slot Jet,'' Int. J. Heat Fluid Flow, **22**, pp. 500–508.

[16] Chen, C.-J., and Jaw, S.-Y., 1998, *Fundamentals of Turbulence Modeling*, Taylor and Francis, Washington, D. C.

[17] Craft, T. J., Graham, L. J. W., and Launder, B. E., 1993, ''Impinging Jet Studies for Turbulence Model Assessment—II. An Examination of the Performance of Four Turbulence Models,'' Int. J. Heat Mass Transfer, **36**, pp. 2685–2697.

[18] Bouainouche, M., Bourabaa, N., Desmet, B., 1997, ''Numerical Study of the Wall Shear Stress Produced by the Impingement of a Plane Turbulent Jet on a Plate,'' Int. J. Numer. Methods Heat Fluid Flow, **7**, pp. 548–564.

[19] Heyerichs, K., and Pollard, A., 1996, ''Heat Transfer in Separated and Impinging Turbulent Flows,'' Int. J. Heat Mass Transfer, **39**, pp. 2385–2400.

[20] Cooper, D., Jackson, C., Launder, B. E., and Liao, G. X., 1993, ''Impinging Jet Studies for Turbulence Model Assessment—I. Flow-field Experiments,'' Int. J. Heat Mass Transfer, **36**, pp. 2675–2684.

[21] Craft, T. J., Launder, B. E., and Suga, K., 1996, ''Development and Application of a Cubic Eddy-Viscosity Model of Turbulence,'' Int. J. Heat Fluid Flow, **17**, pp. 108–115.

[22] Turgeon, E., and Pelletier, D., 2001, ''Verification and Validation of Adaptive Finite Element Method for Impingement Heat Transfer,'' J. Thermophys. Heat Transfer, **15**, pp. 284–292.

[23] Merci, B., Vierendeels, I., DeLange, C., and Dick, E., 2003, ''Numerical Simulation of Heat Transfer of Turbulent Impinging Jets with Two-Equation Turbulence Models,'' Int. J. Numer. Methods Heat Fluid Flow, **13**, pp. 110–132.

[24] Souris, N., Liakos, H., Founti, M., Palyvos, J., and Markatos, N., 2002, ''Study of Impinging Turbulent Jet Flows Using the Isotropic Low-Reynolds Number and the Algebraic Stress Methods,'' Comput. Mech., **28**, pp. 381–389.

[25] Heck, U., Fritsching, K., and Bauckhage, K., 2001, ''Fluid Flow and Heat Transfer in Gas Jet Quenching of a Cylinder,'' Int. J. Numer. Methods Heat Fluid Flow, **11**, pp. 36–49.

[26] Wilcox, D. C., 2002, *Turbulence Modeling For CFD*, DCW Industries, La Cañada, CA.

[27] Park, T. H., Choi, H. G., Yoo, J. Y., and Kim, S. J., 2003, ''Streamline Upwind Numerical Simulation of Two-Dimensional Confined Impinging Slot Jets,'' Int. J. Heat Mass Transfer, **46**, pp. 251–262.

[28] Chen, Q., and Modi, V., 1999, ''Mass Transfer in Turbulent Impinging Slot Jets,'' Int. J. Heat Mass Transfer, **42**, pp. 873–887.

[29] Shih, T.-H., Liou, W. W., Shabbir, A., Yang, Z., and Zhu, J., 1995, ''A New k-ε Eddy-Viscosity Model for High Reynolds Number Turbulent Flows—Model Development and Validation,'' Comput. Fluids, **24(3)**, pp. 227–238.

[30] Abdon, A., and Sunden, B., 2001, ''Numerical Investigation of Impingement Heat Transfer using Linear and Nonlinear Two-Equation Turbulence Models,'' Numer. Heat Transfer, Part A, **40**, pp. 563–578.

[31] Park, T. S., and Sung, H. J., 2001, ''Development of a Near-wall Turbulence Model and Application to Jet Impingement Heat Transfer,'' Int. J. Heat Fluid Flow, **22**, pp. 10–18.

[32] Chen, C.-J., and Jaw, S.-Y., 1998, *Fundamentals of Turbulence Modeling*, Taylor and Francis, Washington, D. C.

[33] Funazaki, K., and Hachiya, K., 2003 ''Systematic Numerical Studies on Heat Transfer and Aerodynamic Characteristics of Impingement Cooling Devices Combined with Pins,'' Proceedings of ASME Turbo Expo 2003, 16–19 June 2003, Atlanta, GA.

[34] Demuren, A. O., 1994, ''Calculations of 3D Impinging Jets in Crossflow with Reynolds Stress Models,'' *Heat Transfer in Turbomachinery*, R. J. Goldstein, D. E. Metzger, A. I. Leontiev, eds., Begell House, New York, pp. 527–540.

[35] Shi, Y., Ray, M. B., and Mujumdar, A. S., 2002, ''Computational Study of Impingement Heat Transfer under a Turbulent Slot Jet,'' Ind. Eng. Chem. Res., **41**, pp. 4643–4651.

[36] Behnia, M., Parneix, S., Durbin, P. A., 1998, ''Prediction of Heat Transfer in an Axisymmetric Turbulent Jet Impinging on a Flat Plate,'' Int. J. Heat Mass Transfer, **41**, pp. 1845–1855.

[37] Behnia, M., Parneix, S., Shabany, Y., and Durbin, P. A., 1999, ''Numerical Study of Turbulent Heat Transfer in Confined and Unconfined Impinging Jets,'' Int. J. Heat Fluid Flow, **20**, pp. 1–9.

[38] Sveningsson, A., and Davidson, L., 2003, ''Assessment of Realizability Constraints and Boundary Conditions in v^2-f Turbulence Models,'' Turbulence, Heat, and Mass Transfer, **4**, pp. 585–592.

[39] Thielen, L., Jonker, H. J. J., and Hanjalić, K., 2003, ''Symmetry Breaking of Flow and Heat Transfer in Multiple Impinging Jets,'' Int. J. Heat Fluid Flow, **24**, pp. 444–453.

[40] Menter, F. R., ''Zonal Two Equation k-ω Turbulence Models for Aerodynamic Flows,'' AIAA-93-2906.

[41] Esch, T., Menter, F., and Vieser, W., 2003, ''Heat Transfer Predictions Based on Two-Equation Turbulence Models,'' TED-AJ03-542, The 6th ASME-JSME Thermal Engineering Joint Conference, 16–20, March 2003.

[42] Goldstein, R. J., and Behbahani, A. I., 1982, ''Impingement of a Circular Jet With and Without Crossflow,'' Int. J. Heat Mass Transfer, **25**, pp. 1377–1382.

[43] Goldstein, R. J., Behbahani, A. I., and Heppelmann, K. K., 1986, ''Streamwise Distribution of the Recovery Factor and the Local Heat Transfer Coefficient to an Impinging Circular Air Jet,'' Int. J. Heat Mass Transfer, **29**, pp. 1227–1235.

[44] Lytle, D., and Webb, B. W., 1994, ''Air Jet Impingement Heat Transfer at low Nozzle-plate Spacings,'' Int. J. Heat Mass Transfer, **37**, pp. 1687–1697.

[45] Meola, C., de Luca, L., and Carlomagno, G. M., 1996, ''Influence of Shear Layer Dynamics on Impingement Heat Transfer,'' Exp. Therm. Fluid Sci., **13**, pp. 29–37.

[46] Mohanty, A. K., and Tawfek, A. A., 1993, ''Heat Transfer Due to a Round Jet Impinging Normal to a Flat Surface,'' Int. J. Heat Mass Transfer, **36**, pp. 1639–1647.

[47] Tawfek, A. A., 1996, ''Heat Transfer and Pressure Distributions of an Impinging Jet on a Flat Surface,'' Heat Mass Transfer, **32**, pp. 49–54.

[48] Wen, M.-Y., and Jang, K.-J., 2003, ''An Impingement Cooling on a Flat Surface by Using Circular Jet with Longitudinal Swirling Strips,'' Int. J. Heat Mass Transfer, **46**(24), pp. 4657–4667.

[49] Chan, T. L., Leung, C. W., Jambunathan, K. J, Ashforth-Frost, S., Zhou, Y., and Liu, M. H., 2002, ''Heat Transfer Characteristics of a Slot Jet Impinging on a Semi-circular Convex Surface,'' Int. J. Heat Mass Transfer, **45**, pp. 993–1006.

[50] Florschuetz, L. W., Truman, C. R., and Metzger, D. E., 1981, ''Streamwise Flow and Heat Transfer Distributions for Jet Array Impingement with Crossflow,'' ASME J. Heat Transfer, **103**, pp. 337–342.

[51] Gori, F., and Bossi, L., 2003, ''Optimal Slot Height in the Jet Cooling of a Circular Cylinder,'' Appl. Therm. Eng., **23**, pp. 859–870.

[52] Huber, A. M., and Viskanta, R., 1994, ''Effect of Jet-Jet Spacing on Convective Heat Transfer to Confined, Impinging Arrays of Axisymmetric Jets,'' Int. J. Heat Mass Transfer, **37**, pp. 2859–2869.

[53] San, J. Y., and Lai, M., 2001, ''Optimum Jet-to-Jet Spacing of Heat Transfer for Staggered Arrays of Impinging Air Jets,'' Int. J. Heat Mass Transfer, **44**, pp. 3997–4007.

[54] Goldstein, R., and Seol, W. S., 1991, ''Heat Transfer to a Row of Impinging Circular Air Jets Including the Effect of Entrainment,'' Int. J. Heat Mass Transfer, **34**, pp. 2133–2147.